Field emission from carbon nanotube fibers in varying anode-cathode gap with the consideration of contact resistance

Peng Zhang,[1,a] S. B. Fairchild,[2] T. C. Back,[2] and Yi Luo[1]
[1]*Department of Electrical and Computer Engineering, Michigan State University, East Lansing, Michigan 48824-1226, USA*
[2]*Materials and Manufacturing Directorate, Air Force Research Laboratory, WPAFB, Ohio 45433, USA*

(Received 11 October 2017; accepted 20 November 2017; published online 4 December 2017; corrected 16 March 2018; 26 March 2018)

This paper studies field emission (FE) from a single carbon nanotube (CNT) fiber with different anode-cathode (AK) gap distances. It is found that the field enhancement factor depends strongly on the finite AK gap distance, due to the combination of geometrical effects and possible fiber morphology change. The geometrical effects of AK gap distance on the field enhancement factor are confirmed using COMSOL simulations. The slope drop in the Fowler-Northeim (FN) plot of the FE data in the high voltage is related to the electrical contact resistance between the CNT fiber and the substrate. It is found that even a small series resistance to the field emitter (<30% of the emission gap impedance) can strongly modify the FE characteristics in the high voltage regime, inducing a strong deviation from the linear FN plot.
https://doi.org/10.1063/1.5008995

Field emission (FE) cathodes have attracted extensive interests due to their wide range of applications, such as in high power microwave devices,[1–3] novel x-ray sources,[4] accelerators,[5] and vacuum nanoelectronics.[6–8] Carbon materials, such carbon nanotube (CNT) fibers,[9–15] have demonstrated promising properties for their use as field emitters, due to their large aspect ratios, and high electrical and thermal conductivities.

One of the key parameters to characterize field emission is the field enhancement factor, typically extracted from the Fowler-Northeim (FN) plot[16,17] of the measured current-voltage (I-V) curves. Many factors contribute to the effective field enhancement factor, and therefore the FN characteristics of the field emitters, such as material properties and geometrical shape of the emitter. Electric field screening by the proximity of neighboring emitters is found to have a profound effect on the field enhancement factor of the cathode.[18–20] Recently, it is shown that field enhancement factor strongly depends on the finite anode-cathode gap distance when the emitter tip-to-anode distance is comparable to or smaller than the emitter height.[8]

In this paper, we study the FE characteristics of a CNT fiber emitter in different anode-cathode (AK) gap distances. We show that the field enhancement factor depends strongly on the finite AK gap distance, due to the combination of geometrical effects and possible change in fiber morphology. The geometrical effects of AK gap distance on the field enhancement factor are confirmed using COMSOL simulations. We show the slope drop in FN plot of the FE data in the high voltage is related to the electrical contact resistance between the CNT fiber and the base.

The CNT fiber was fabricated by a wet spinning technique from bulk-grown carbon nanotubes dispersed in superacides.[15] The FE current data was measured from the tip of a razor cut CNT fiber in an ultrahigh vacuum chamber whose base pressure was 5.0×10^{-9} Torr. The fiber emitter has

[a]Corresponding author: pz@egr.msu.edu

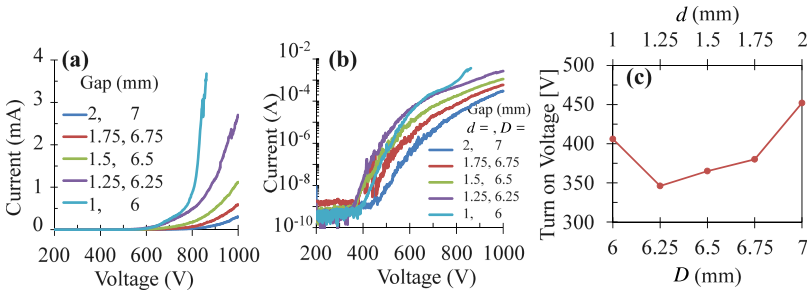

FIG. 1. Current-voltage (*I*-*V*) curves for the CNT fiber at different tip-to-anode distance *d* in (a) linear scale, and (b) semi-log scale. (c) The turn on voltage as a function of the gap distance. The anode-cathode (AK) gap distance $D = h + d$, where $h = 5$ mm is the emitter height, and *d* is set at 2, 1.75, 1.5, 1.25, 1 mm.

a radius of $r = 5$ μm and a height of $h \approx 5$ mm, which was mounted to a stainless steel sample holder with silver paint, which grounded the fiber. A stainless steel anode probe tip (7 mm diameter) was aligned with the CNT fiber, which was monitored by using two orthogonally situated cameras looking through two different windows on the chamber. One camera was equipped with a long working distance objective to accurately determine the emitter tip-to-anode distance *d*. The distance *d* was varied with integrated stepper motors capable of 2.5 μm travel per step. The voltage applied across the AK gap was controlled with a Keithley 2410 source meter. For a given distance *d*, the external voltage was increased from 200 to the maximum of 1000 V at a rate of 1 V per 10 s and the FE current was recorded at each voltage step using LabView control. Once a complete voltage sweep was carried out, the tip-to-anode distance *d* was reduced, and the data acquisition process was repeated. Five different experimental runs were performed for $d = 2$, 1.75, 1.5, 1.25, and 1 mm.

Figure 1 shows the FE current data from the single CNT fiber at different values of the AK gap distance *D*, which is the sum of the fiber height $h = 5$ mm and the tip-to-anode distance *d*. In general, as *D* decreases, the emission current increases for a given external voltage V_{ext}. This is due to the increased cathode electric field ($\sim V_{ext}/D$). More importantly, as will be discussed below, the effective electric field enhancement factor (β_{eff} in Eq. (1)) near the emission tip is largely increased as the gap distance *D* decreases, especially when the fiber tip-to-anode distance *d* is smaller than fiber height *h*, $d \leq h$, as recently studied by Lin *et al.*[8] It is clear that in general the turn on voltage also decreases as the gap distance *D* decreases, as shown in Fig. 1c, which is also due to the increased cathode electric field and the increased field enhancement factor for a smaller AK gap. Note the turn on voltage here is defined as the one corresponding to the upward bending of the curve in the semi-log I-V plots (Fig. 1b) or in the FN plot (Fig. 2a). The dependence of the turn on voltage on AK gap distance agrees with previous studies.[21,22]

As shown in Figs. 1(b) and 1(c), the *I*-*V* curve for $d = 1$ mm ($D = 6$ mm) is distinctive, with a larger turn on voltage and an upper bend near $V_{ext} = 780$ V. We attribute this to the possible conditioning or damage of the CNT fiber during the previous run with $d = 1.25$ mm. In fact, for $d = 1.25$ mm, it was observed that there was a flash near the emitter tip when the applied voltage was increased to 920 V, and plasma was formed at the fiber tip at 935 V. The presence of plasma likely induced certain damage or conditioning to the CNT fiber, thus showing a different *I*-*V* characteristics at the subsequent run of $d = 1$ mm. As shown in Fig. 1(a), there is a sudden drop in the emission current around $V_{ext} = 980$ V for $d = 1.25$ mm, and around $V_{ext} = 850$ V for $d = 1$ mm. This kind of sudden drop is attributed to the self-heating effects, which can lead to a sudden failure to emit for some of the CNTs forming the fiber.[13,23] For $d = 1$ mm, the fiber failed to emit entirely, shortly after applying the maximum voltage of 1000 V.

Figure 2(a) show the FN plot of the measured *I*-*V* curves in Fig. 1. For FN FE, the current-gap voltage characteristics should be well fitted by the FN equation[16,17,24]

$$I(\mathrm{A}) = S_{eff} A \left(\beta_{eff} \frac{V_g}{D}\right)^2 e^{-\frac{B}{\beta_{eff} V_g / D}}, \tag{1}$$

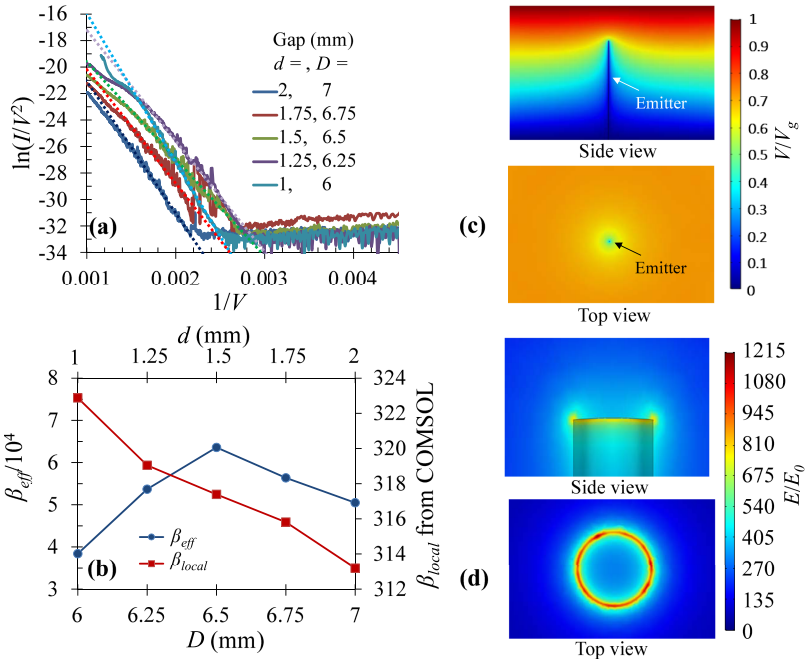

FIG. 2. (a) FN plot of the FE data in Fig. 1. Dashed lines are straight lines fitted to the FN data. (b) The effective field enhancement factor β_{eff} as a function of the AK gap distance D (and the tip-to-anode distance d), extracted from the slope of the curves in (a) according to Eq. (1). Also plotted in (b) is the local field enhancement factor $\beta_{local} = E_{local}/E_0$, which is the ratio of the local vacuum electric field at the center of the top surface of the tip E_{local} over the uniform electric field far away from the tip $E_0 = V_g/D$, obtained from COMSOL electrostatic simulations. (c) Potential profile and (d) electric field profile near the tip of the emitter for the case of d = 1.75 mm. In the simulation, the electric field is calculated by assuming perfect conducting cathode (including the cylindrical tip) and anode, with the emitter dimensions of the CNT fiber used in experiments, of height h = 5 mm, radius r = 5 μm.

where $A = 1.54 \times 10^{-6}/W$, $B = 6.83 \times 10^9 W^{3/2}$, S_{eff} is the effective emission area (m^2) of the fiber, W is the work function (in eV) of the emitting surface, β_{eff} is the effective field enhancement factor, $D = h + d$ is the gap distance (in m) between the anode and the base of the CNT fiber cathode, which is the sum of the fiber length h and the fiber tip-to-anode distance d, and V_g is the gap voltage. In the FN plot, Equation (1) yields a straight line when plotted as $\ln(I/V_g^2)$ vs $1/V_g$, with the slope of $-BD/\beta_{eff}$. By assuming the gap voltage is the same as the external applied voltage, $V_g = V_{ext}$ (i.e. no series resistance to the emitter is assumed), the measured FN data can be fitted by a straight line when the applied voltage is small, as shown in Fig. 2(a). From the slope of these linear fitting, the effective field enhancement factor β_{eff} is extracted, as shown in Fig. 2(b). In all the curve fitting, a constant work function of W = 4.8 eV is assumed for the CNT fiber emitter.

For a given fixed CNT fiber length (h = 5 mm), when the gap distance D decreases, the ratio D/h decreases, which will lead to an rapid increase in both the local and effective field enhancement factor for $D/h < 2$. As studied in Ref. 8, this is purely a geometrical effect. Electrostatic simulations using COMSOL[25] on the local vacuum electric field at the tip center of the emitter confirms this scaling, also shown in Fig. 2(b). The potential and electric field profiles are shown in Figs. 2(c)–(d). It is important to note that the effective field enhancement factor β_{eff} extracted from the FN plot according to Eq. (1) is a different quantity from the local field enhancement factor $\beta_{local} = E_{local}/E_0$, which is simply the ratio of the local vacuum electric field at the center of the tip E_{local} over the uniform electric field far away from the tip $E_0 = V_g/D$. Nevertheless, β_{eff} and β_{local} show similar scaling as a function of dimensions. The observed trend of increasing field enhancement factor with decreasing AK gap distance is in agreement with previous computational modeling[26] and experiments on CNT field emitters.[27] The drop of effective field enhancement factor for d = 1 mm and d = 1.25 mm is due to the possible change in the fiber morphology with the decreased gap, as noted in Refs. 13 and 14. The above mentioned flash and plasma observed at the larger applied field at d = 1.25 mm may have

destroyed some of the sharper features on the CNT fiber, leaving CNTs with lower field enhancement factors. As observed previously,[14] after the plasma forms at the fiber tip, the fiber tip "plumes" out, thus the field enhancement factor decreases because the fiber tip is less pointy. This would also explain the increased turn-on voltage for FE the last run at d = 1 mm (Fig. 1(b)). Note that some of the previous studies (Ref. 28 and reference therein) also reported a growing field enhancement factor with increasing AK distance for self-catalyzed GaAs nanowires. The complicated dependence of the field enhancement factor with AK distance might therefore be the result of two competing effects: geometrical effects and material effects.

When the applied voltage is high, the measured I-V curves in the FN plot cannot be fitted by straight lines, but with reduced slopes, as shown in Fig. 2(a). The saturation region of the FN plot has been extensively studied.[29–33] We will show that this slope drop is probably due to the finite series resistance in the circuit of the field emitter.[29] In FE system, there is always series resistance R to the emitter when the circuit is closed. Thus, the gap voltage V_g is related to the external applied voltage V_{ext} as,

$$V_{ext} = V_g + IR = I(Z + R), \tag{2}$$

where R is the total series resistance to the emitter, I is the emission current, and Z is the lumped circuit element of impedance used to represent the field emitter gap. By solving the coupled equations (1) and (2), the results are fitted to the measured data, as shown in Fig. 3(a). The corresponding series resistance R and the emission gap impedance Z are shown in Fig. 3(b). Note that we have used the same β_{eff} as in Fig. 2, since the voltage drop across R in the low voltage regime is negligible (i.e. $V_{ext} \cong V_g$). As the gap distance D decreases, the emission gap impedance $Z = V_g/I$ drops significantly, because the emission current I increases rapidly. The series resistance R is on the order of $10^5\Omega$, with a slight decrease as D decreases. It is important to note that the ratio of the series resistance to the gap impedance is very small, $R/Z < 0.3$ at the maximum (c.f. Fig. 3(b)), which, however, has a strong effect on the field emission characteristics, making it deviant from a straight line in the FN plot in the high voltage regime.

The total series resistance R consists of resistance of various parts of the circuit,

$$R = R_{CNT\ fiber} + R_{substrate} + R_{contact} + R_{ext}, \tag{3}$$

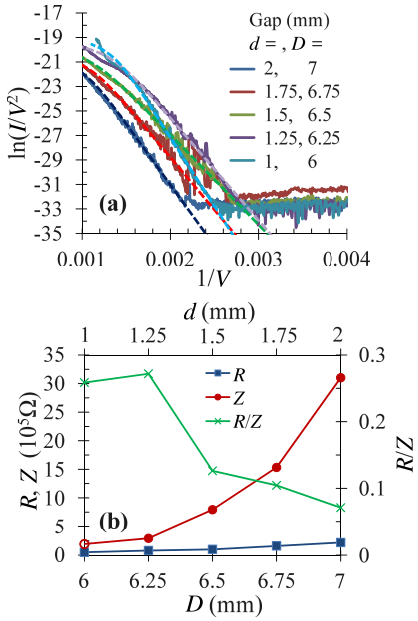

FIG. 3. (a) Curve fitting (dashed lines) to the FE data (solid lines) by including the effects of a series resistance, calculated by solving the coupled Eqs. (1) and (2), and (b) the corresponding series resistance R and the gap impedance $Z = V_g/I$ as a function of AK gap distance D (and the tip-to-anode distance d). The open symbol for Z at d = 1 mm is calculated by using the theoretically extrapolated current at 1000V. Also shown is the ratio R/Z at different gap distance.

where the resistance of the substrate $R_{substrate}$ and of external circuit R_{ext} are negligible since the stainless steel substrate and electrodes are highly conductive (with resistivity of $7.2 \times 10^{-7}\Omega$m),[34] the resistance of the CNT fiber $R_{CNT\,fiber} = \rho_{CNT\,fiber} h/\pi r^2 = 112\ \Omega$, with the assumption of CNT fiber's resistivity[14] being $\rho_{CNT\,fiber} = 1.75 \times 10^{-6}\Omega$m, length $h = 5$ mm, and radius $r = 5\mu$m, and $R_{contact}$ is the contact resistance between the CNT fiber and the substrate. Therefore, the dominate component of the series resistance in Eq. (3) is the contact resistance, $R_{contact} = R_{constriction} + R_{interface}$, where the constriction resistance $R_{constriction}$ is due to the constriction of current flow lines near the base of the field emitter, and $R_{interface}$ is the interface resistance.[35–37] The rough estimate of constriction resistance[35] is $R_{constriction} \approx \rho_{base}/4r = 7.2 \times 10^{-7}\Omega\text{m}/(4 \times 5\text{ mm}) = 4 \times 10^{-5}\Omega$, which indicates the high contact resistance (therefore series resistance) is due to the interface resistance (i.e. $R \approx R_{interface}$). Possible contribution to the interface resistance include resistive foreign contaminants (e.g. oxides) and tunneling resistance between the CNT fiber and the stainless steel sample holder, with the presence of nanoscale vacuum or oxide gap between them.[38,39] In fact, the slight decrease of the interface resistance (therefore series resistance R in Fig. 3(b)) with decreasing AK gap D is expected, if it is dominated by the interface tunneling resistance, which decreases as the current level increases.[39] The interface resistance of the order of $10^5\Omega$ (c.f. Fig. 3(b)) is smaller than the typical value of contact resistance for CNT (of the order of MΩ), e.g. in Ref. 30, indicating good electrical contact of CNT fiber to the substrate in the current experiment.

Note that the slope drop in the high voltage regime in the FN plot is usually attributed to space charge effects,[13,40,41] or outgassing of the field emitter.[12] When the classical Child-Langmuir law $I_{CL} \propto V_g^{3/2}$ is displayed in the FN plot, as $\ln(I/V_g^2)$ vs $1/V_g$, there would be a positive slope of $V_g/2$ (e.g. in Ref. 13). This is not the case in the present emission data, as shown in Figs. 2(a) and 3(a). Thus, it is unlikely that space charge effects are the major cause of the slope drop. It was shown previously that outgassing is significantly reduced after the initial run and is negligible at higher voltages.[12] If outgassing is present to change the surface chemistry of the emitter, due to either desorption of the gas adsorbates, or the back bombardment from the ionized desorbed species, the FN data typically manifests hysteresis behavior.[12,13] However, it is found that the I-V curves are symmetric when sweeping the voltage up and down (not shown) for the $d = 1.75$ mm case. Therefore, the slope drop in the FN plots of the present FE data is most likely due to the electrical contact resistance between the CNT fiber and the substrate.

In summary, we have studied field emission from a single CNT fiber with different AK gap distance. The dependence of the field enhancement factor on the gap distance is analyzed, by the consideration of both geometrical effects and possible fiber morphology change. The pure geometrical effects predicts that both the effective field enhancement factor and the local enhancement factor increase with decreasing AK gap distance, which is confirmed by numerical simulations. The decrease of the effective field enhancement factor at the small gap distance characterized is attributed to the possible fiber morphology change during the previous runs, where the sharp features contributing to field emission may be damaged by the presence of flash and plasmas near the emitter tip. The slope drop in the high voltage regime of the FN plot is studied. The FN plot is fitted very well by including a series resistance in the FN equation. The major contribution of the series resistance is thought to be from the electrical contact resistance between the CNT fiber and the substrate. Our study suggests that further improving the contact resistance, along with the electrical conductivity of the CNT fiber, would be important to achieve high field emission current. As contact resistance between the CNT fiber and the substrate is typically much higher than the resistance of the fiber itself, the majority of the Joule heating is deposited at the contact region, leading to possible degradation and to the eventual failure of the cathodes.[42] Future work will involve testing of FE at higher voltages up to 100 kV, where the improvement of contact resistance between the CNT fiber and the substrate will become even more important to the cathode lifetime. Future studies also include more detailed electron tunneling models with non-metals, and direct measurement of the work function.

ACKNOWLEDGMENTS

This material is based upon work supported by the Air Force Office of Scientific Research under award number FA9550-14-0309 through a subcontract from the University of Michigan, by the Air

Force Office of Scientific Research YIP award number FA9550-18-1-0061, and by the Air Force Office of Scientific Research under award number FA9550-17RXCOR428.

[1] J. H. Booske, Phys. Plasmas 1994-Present **15**, 055502 (2008).
[2] D. Shiffler, T. K. Statum, T. W. Hussey, O. Zhou, and P. Mardahl, in *Mod. Microw. Millim. Wave Power Electron.* (IEEE, Piscataway, NJ, 2005), p. 691.
[3] C. M. Armstrong, IEEE Spectr. Technol. Eng. Sci. News (2015).
[4] D. Chen, X. Song, Z. Zhang, Z. Li, J. She, S. Deng, N. Xu, and J. Chen, Appl. Phys. Lett. **107**, 243105 (2015).
[5] P. Hommelhoff, Y. Sortais, A. Aghajani-Talesh, and M. A. Kasevich, Phys. Rev. Lett. **96**, 077401 (2006).
[6] A. Evtukh, H. Hartnagel, O. Yilmazoglu, H. Mimura, and D. Pavlidis, *Vacuum Nanoelectronic Devices: Novel Electron Sources and Applications*, 1 edition (Wiley, Chichester, West Sussex, United Kingdom, 2015).
[7] P. Zhang, A. Valfells, L. K. Ang, J. W. Luginsland, and Y. Y. Lau, Appl. Phys. Rev. **4**, 011304 (2017).
[8] J. Lin, P. Y. Wong, P. Yang, Y. Y. Lau, W. Tang, and P. Zhang, J. Appl. Phys. **121**, 244301 (2017).
[9] D. A. Shiffler, M. J. LaCour, M. D. Sena, M. D. Mitchell, M. D. Haworth, K. J. Hendricks, and T. A. Spencer, IEEE Trans. Plasma Sci. **28**, 517 (2000).
[10] D. Shiffler, S. Fairchild, W. Tang, B. Maruyama, K. Golby, M. LaCour, M. Pasquali, and N. Lockwood, IEEE Trans. Plasma Sci. **40**, 1871 (2012).
[11] W. Tang, D. Shiffler, K. Golby, M. LaCour, and T. Knowles, J. Vac. Sci. Technol. B **30**, 061803 (2012).
[12] P. T. Murray, T. C. Back, M. M. Cahay, S. B. Fairchild, B. Maruyama, N. P. Lockwood, and M. Pasquali, Appl. Phys. Lett. **103**, 053113 (2013).
[13] M. Cahay, P. T. Murray, T. C. Back, S. Fairchild, J. Boeckl, J. Bulmer, K. K. K. Koziol, G. Gruen, M. Sparkes, F. Orozco, and W. O'Neill, Appl. Phys. Lett. **105**, 173107 (2014).
[14] S. B. Fairchild, J. Boeckl, T. C. Back, J. B. Ferguson, H. Koerner, P. T. Murray, B. Maruyama, M. A. Lange, M. M. Cahay, N. Behabtu, C. C. Young, M. Pasquali, N. P. Lockwood, K. L. Averett, G. Gruen, and D. E. Tsentalovich, Nanotechnology **26**, 105706 (2015).
[15] N. Behabtu, C. C. Young, D. E. Tsentalovich, O. Kleinerman, X. Wang, A. W. K. Ma, E. A. Bengio, R. F. ter Waarbeek, J. J. de Jong, R. E. Hoogerwerf, S. B. Fairchild, J. B. Ferguson, B. Maruyama, J. Kono, Y. Talmon, Y. Cohen, M. J. Otto, and M. Pasquali, Science **339**, 182 (2013).
[16] R. H. Fowler and L. Nordheim, Proc. R. Soc. Lond. Ser. A **119**, 173 (1928).
[17] A. Modinos, Solid-State Electron. **45**, 809 (2001).
[18] W. Tang, D. Shiffler, and K. L. Cartwright, J. Appl. Phys. **110**, 034905 (2011).
[19] W. Tang, D. Shiffler, K. Golby, M. LaCour, and T. Knowles, J. Vac. Sci. Technol. B Nanotechnol. Microelectron. Mater. Process. Meas. Phenom. **32**, 052202 (2014).
[20] J. R. Harris, K. L. Jensen, J. J. Petillo, S. Maestas, W. Tang, and D. A. Shiffler, J. Appl. Phys. **121**, 203303 (2017).
[21] A. Di Bartolomeo, A. Scarfato, F. Giubileo, F. Bobba, M. Biasiucci, A. M. Cucolo, S. Santucci, and M. Passacantando, Carbon **45**, 2957 (2007).
[22] M. Passacantando, F. Bussolotti, S. Santucci, A. D. Bartolomeo, F. Giubileo, L. Iemmo, and A. M. Cucolo, Nanotechnology **19**, 395701 (2008).
[23] F. Antoulinakis, D. Chernin, P. Zhang, and Y. Y. Lau, J. Appl. Phys. **120**, 135105 (2016).
[24] R. G. Forbes, J. Vac. Sci. Technol. B Microelectron. Nanometer Struct. Process. Meas. Phenom. **17**, 526 (1999).
[25] Https://Www.comsol.com/ (n.d.).
[26] C. J. Edgcombe and U. Valdrè, J. Microsc. **203**, 188 (2001).
[27] J.-M. Bonard, K. A. Dean, B. F. Coll, and C. Klinke, Phys. Rev. Lett. **89**, 197602 (2002).
[28] F. Giubileo, A. Di Bartolomeo, L. Iemmo, G. Luongo, M. Passacantando, E. Koivusalo, T. V. Hakkarainen, and M. Guina, Nanomaterials **7**, 275 (2017).
[29] J. W. Luginsland, A. Valfells, and Y. Y. Lau, Appl. Phys. Lett. **69**, 2770 (1996).
[30] J.-M. Bonard, C. Klinke, K. A. Dean, and B. F. Coll, Phys. Rev. B **67**, 115406 (2003).
[31] R. G. Forbes, Appl. Phys. Lett. **110**, 133109 (2017).
[32] E. Minoux, O. Groening, K. B. K. Teo, S. H. Dalal, L. Gangloff, J.-P. Schnell, L. Hudanski, I. Y. Y. Bu, P. Vincent, P. Legagneux, G. A. J. Amaratunga, and W. I. Milne, Nano Lett. **5**, 2135 (2005).
[33] M. Bachmann, F. Dams, F. Düsberg, M. Hofmann, A. Pahlke, C. Langer, R. Ławrowski, C. Prommesberger, R. Schreiner, P. Serbun, D. Lützenkirchen-Hecht, and G. Müller, J. Vac. Sci. Technol. B Nanotechnol. Microelectron. Mater. Process. Meas. Phenom. **35**, 02C103 (2016).
[34] W. M. Haynes, *CRC Handbook of Chemistry and Physics*, 94th Edition, 94 edition (CRC Press, Boca Raton (Fla.); London; New York, 2013).
[35] P. Zhang and Y. Y. Lau, J. Appl. Phys. **108**, 044914 (2010).
[36] P. Zhang, Y. Y. Lau, and R. M. Gilgenbach, J. Appl. Phys. **109**, 124910 (2011).
[37] P. Zhang and Y. Y. Lau, Appl. Phys. Lett. **104**, 204102 (2014).
[38] J. G. Simmons, J. Appl. Phys. **34**, 1793 (1963).
[39] P. Zhang, Sci. Rep. **5**, 9826 (2015).
[40] Y. Y. Lau, Y. Liu, and R. K. Parker, Phys. Plasmas 1994-Present **1**, 2082 (1994).
[41] Y. Feng and J. P. Verboncoeur, Phys. Plasmas 1994-Present **13**, 073105 (2006).
[42] L. T. Williams, V. S. Kumsomboone, W. J. Ready, and M. L. R. Walker, IEEE Trans. Electron Devices **57**, 3163 (2010).